JVI Journals.ASM.org

Structure and Functional Analysis of the Host Recognition Device of Lactococcal Phage Tuc2009

Barry Collins,[a] Cecilia Bebeacua,[b,c] Jennifer Mahony,[a] Stéphanie Blangy,[b,c] François P. Douillard,[a]* David Veesler,[b,c]* Christian Cambillau,[b,c] Douwe van Sinderen[a,d]

Department of Microbiology, University College Cork, Cork, Ireland[a]; Aix-Marseille Université, Architecture et Fonction des Macromolécules Biologiques, Campus de Luminy, Marseille, France[b]; Centre National de la Recherche Scientifique, Architecture et Fonction des Macromolécules Biologiques, UMR 6098, Campus de Luminy, Marseille, France[c]; Alimentary Pharmabiotic Centre, University College Cork, Cork, Ireland[d]

Many phages employ a large heteropolymeric organelle located at the tip of the tail, termed the baseplate, for host recognition. Contrast electron microscopy (EM) of the lactococcal phage Tuc2009 baseplate and its host-binding subunits, the so-called tripods, allowed us to obtain a low-resolution structural image of this organelle. Structural comparisons between the baseplate of the related phage TP901-1 and that of Tuc2009 demonstrated that they are highly similar, except for the presence of an additional protein in the Tuc2009 baseplate ($BppA_{Tuc2009}$), which is attached to the top of the Tuc2009 tripod structure. Recombinantly produced Tuc2009 or TP901-1 tripods were shown to bind specifically to their particular host cell surfaces and are capable of almost fully and specifically eliminating Tuc2009 or TP901-1 phage adsorption, respectively. In the case of Tuc2009, such adsorption-blocking ability was reduced in tripods that lacked $BppA_{Tuc2009}$, indicating that this protein increases the binding specificity and/or affinity of the Tuc2009 tripod to its host receptor.

Bacterial viruses (bacteriophages, or phages) of the order *Caudovirales* possess a tail that recognizes the host and ensures genome delivery upon infection. This host recognition event is mediated through binding of the tip of the tail to either a protein receptor or a carbohydrate moiety located in or on the cell envelope (1–3). Well-characterized examples of bacteriophages with protein receptors include coliphages lambda and T5, which recognize LamB and FhuA, respectively, both located on the surface of the *Escherichia coli* cell envelope (4–7), and *Bacillus* phage SPP1, which recognizes YueB at the cell surface (8, 9). An alternative cell binding approach by prototype bacteriophage T4 follows a two-step process whereby the T4 long tail fibers first reversibly bind lipopolysaccharide (LPS) or OmpC (10–13), causing a conformational change in the baseplate, which then allows irreversible binding of the short tail fibers of the baseplate to LPS (14). In the case of carbohydrate-dependent host recognition, phages appear to employ a so-called baseplate, a large heteropolymeric proteinaceous organelle, in order to ensure efficient and host-specific binding (15, 16). The study of saccharidic phage receptors is still in its infancy but differs from the protein receptor model in that, due to the relative weakness of an individual carbohydrate-protein interaction, phage binding to a host is consolidated typically by a large number of receptor binding proteins (RBPs) in the phage baseplate (17, 18). The baseplate structures have only relatively recently been recognized as host recognition devices and are of particular interest among phages of *Lactococcus lactis*.

L. lactis is a Gram-positive bacterium extensively employed as a starter culture in dairy fermentations. Due to its extensive and global industrial exploitation, many phages infecting various strains of the bacterium have been isolated and described. These phages have been grouped into 10 different species based on DNA homology and morphology (19). Among these, representatives of the c2, P335, and 936 species are the most commonly encountered phages in the dairy environment, where members of the c2 species are known to recognize a proteinaceous receptor, while characterized members of the other two species possess a distinct baseplate and thus are thought to bind to a saccharidic receptor (20). A striking feature of these phages, in particular the 936 and P335 species, is their narrow host range: each phage infects a small number of hosts with exquisite specificity among hundreds of different *L. lactis* strains (21–23). The exact molecular nature of the saccharidic receptors has long been a matter of speculation. While it was first proposed that they are lipoteichoic acids (24), the limited diversity of these phosphosaccharides was at odds with the observed host recognition specificity of lactococcal phages. The discovery of the so-called "pellicle" layer, which consists of an extracellular phosphopolysaccharide and which was shown to be required for infection of a 936-type phage (25), presented the possibility of a phage receptor that is sufficiently different between strains to be compatible with the particular host specificity of lactococcal phages.

To understand the molecular basis of lactococcal-phage host recognition, we previously performed structural studies of the RBPs of representatives of the two major lactococcal-phage species, the 936 type (for phages p2 and bIL170) and the P335 type (for phage TP901-1) (17, 24, 26, 27). We also determined the atomic structures of the baseplate of phage p2 (16) and that of phage TP901-1 (15, 18), revealing striking differences in their host recognition mechanisms (15, 16, 28, 29). The p2 baseplate under-

Received 8 April 2013 Accepted 16 May 2013
Published ahead of print 22 May 2013
Address correspondence to Douwe van Sinderen, d.vansinderen@ucc.ie, or Christian Cambillau, cambillau@afmb.univ-mrs.fr.
* Present address: François P. Douillard, Department of Veterinary Biosciences, University of Helsinki, Helsinki, Finland; David Veesler, Department of Molecular Biology, Scripps Research Institute, La Jolla, California, USA.
B.C. and C.B. contributed equally to this work.

doi:10.1128/JVI.00907-13

TABLE 1 Bacterial strains, phages, and plasmids used in this study

Strain, phage, or plasmid[a]	Relevant feature	Reference
L. lactis strains		
NZ9000	*L. lactis* carrying *nisRK* on the chromosome	48
UC509.9	Host for Tuc2009; UC509.9 cured of prophage	49
3107	Host for TP901.1	50
Phages		
Tuc2009	Phage isolated from *L. lactis* subsp. *cremoris* UC509	49
TP901.1	Phage isolated from *L. lactis* subsp. *cremoris* 901-1	50
Plasmids		
pTX8048	pNZ8048 derivative for generating thioredoxin fusions; contains a His tag cloned in frame	32
pTX8049	pNZ8048 derivative for generating thioredoxin fusions	32
pNZ8048	*L. lactis* expression vector containing the *nisp* promoter; Cm^r	48
(1) pTX8048-UAL	pTX8048 encoding Tuc2009 BppU, BppA, and BppL as an operon	32
(2) pTX8048-UA	pTX8048 encoding Tuc2009 BppU and BppA as an operon	This study
(3) pTX8048-UL	pTX8048 encoding Tuc2009 BppU and BppL as an operon	This study
(4) pTX8048-AL	pTX8048 encoding Tuc2009 BppA and BppL as an operon	This study
(5) pTX8049-UctAL	pTX8049 encoding Tuc2009 BppUct, BppA and BppL as an operon; TEV cleavage site	This study
(6) pTX8049-UctL	pTX8049 encoding Tuc2009 BppUct and BppL as an operon; TEV cleavage site	This study
(7) pTX8048-U-24AL	pTX8048 encoding Tuc2009 BppU-24, BppA and BppL as an operon	This study
(8) pTX8049-Uct-24AL	pTX8049 encoding Tuc2009 BppUct-24, BppA and BppL as an operon; TEV cleavage site	This study
(9) pTX8048-TP901.1UL	pTX8048 encoding TP901.1 BppU and BppL as an operon	This study

[a] The numbers in parentheses correspond to the expression constructs in Fig. 1B.

goes a dramatic conformational change as a prerequisite for host recognition, an event that is catalyzed by Ca^{2+} (16). In contrast, the TP901-1 baseplate is maintained in a "ready-to-use" conformation, and infection by this phage is not dependent on Ca^{2+} (29). The established baseplate models of these 936 and P335 phages possess a common architecture, consisting of six receptor binding subunits formed around a central core (15, 16). In the case of TP901-1, a prototype P335 phage, the central core consists of a Dit hexamer that holds six receptor binding subunits, also called tripods due to their shape, which are each composed of three BppU and nine BppL protein monomers (18). Since the BppL protein represents the RBP, it follows that TP901-1's baseplate possesses 54 RBPs, each of which capable of interacting with a carbohydrate receptor.

An "in-solution" baseplate model was previously established for phage Tuc2009 (30), and in the current work, we utilized electron microscopy (EM) to obtain a low-resolution structural image of the Tuc2009 baseplate and tripods, which, relative to TP901-1, harbors an additional protein, and to demonstrate binding of recombinantly produced phage tripods to their specific host and their ability to competitively and specifically exclude phage particles from host adsorption.

MATERIALS AND METHODS

Bacterial strains and growth conditions. The bacterial strains used in this study are listed in Table 1. *L. lactis* was cultured in GM17 (M17 broth; Oxoid, United Kingdom) with 0.5% (wt/vol) D-glucose (Sigma, St. Louis, MO, USA) at 30°C under static conditions. *L. lactis* transformants were selected on GM17 agar plates supplemented with 5 μg/ml chloramphenicol (Sigma, United Kingdom). Where nisin was required for controlled gene induction, we used Nisaplin powder (2.5% nisin; Danisco, United Kingdom) dissolved in sterile water at a final concentration of 40 ng/ml.

Cloning. The primers used for amplification and cloning purposes were purchased from Eurofins MWG (Germany). PCR amplifications were carried out using KOD high-fidelity DNA polymerase (Novagen, United Kingdom), restriction enzymes were obtained from Roche (Germany), and T4 DNA ligase was purchased from Promega. Phage template DNA was obtained by infecting *L. lactis* UC509.9 with Tuc2009, followed after 1 h by total genomic DNA extraction (31). In order to generate protein pairings for all the possible combinations of Tuc2009 baseplate tripod proteins ($BppUA_{Tuc2009}$, $BppUL_{Tuc2009}$, $BppAL_{Tuc2009}$, and $BppUAL_{Tuc2009}$), PCR products encompassing the genes for each combination were digested with BamHI and SpeI and cloned into the similarly restricted expression vector pTX8049 or pTX8048 (32). The adjacent genes encoding $BppU_{Tuc2009}$ and $BppA_{Tuc2009}$ were amplified using the primers UAL_F (AGCAGCGGATCCATGACAGAACATTTTATAAC) (underlining indicates a BamHI restriction site) and UA_R (AGCAGC**ACTAGT**TTATTTGGGTAGTGTTGTTT) (underlining and boldface indicate an SpeI restriction site) and cloned into pTX8048, while genes specifying $BppA_{Tuc2009}$ and $BppL_{Tuc2009}$ were amplified using UAL_R (AGCAGC**ACTAGT**TTAATTCCGATAAAGTTTTACAATC) and AL_F (AGCAGCGGATCCATGGCAGATAAAAATTATT) and cloned into pTX8048. A splicing-by-overlap-extension (SOE) (33) strategy was utilized to generate a construct that encoded $BppU_{Tuc2009}$ and $BppL_{Tuc2009}$. Primers UAL_F and U_SOE (*TTTATTCTCCTATTTCTA*TTATCCCCC GTTTTCCCACGAAA) (italics indicate overhang used for SOE) were used to amplify the $BppU_{Tuc2009}$-encoding gene, while the primer combination L_SOE (*TAGAAATAGGAGAATAAA*ATGGCTGAATTAACTAA AATTAC) and UAL_R generated the coding region for BppL. The last two PCR products harbored complementary overhangs and were employed for this purpose as a combined template to generate a $bppUL_{Tuc2009}$-specifying DNA region by amplification using the primer combination UAL_F and UAL_R, after which the SOE product was cloned into pTX8048.

A variant of the Tuc2009 $BppUAL_{Tuc2009}$ tripod in which only the C-terminal part of $BppU_{Tuc2009}$ was present, designated $BppUct_{Tuc2009}$, was produced (encompassing amino acids [aa] 194 to 322 of $BppU_{Tuc2009}$). In order to generate this $BppUctAL_{Tuc2009}$-encoding construct, the relevant DNA was amplified using primers UCt_F (AGCGGATCC**CACCATCATCATCATC ATT**CTTCTGGgaaaac ctgtacttccagggttctAGCGGATTTAATGTAGTAA TTGAGC) (the polyhistidine tag is in boldface, while lowercase indicates a TEV protease cleavage site) and UAL_R, after which the resulting amplicon was cloned into pTX8049. The BppUCt primer was designed so as

to generate a thioredoxin fusion product of the C-terminal 129 amino acids of BppU. The BppUctL$_{Tuc2009}$-encoding construct was generated, utilizing pTX8048-UL as a template; primers UCt_F and UAL_R were used to generate a BppUctL$_{Tuc2009}$-specifying amplicon, which was cloned into pTX8049.

A derivative of BppU$_{Tuc2009}$ with the C-terminal 24 amino acids removed (BppU-24$_{Tuc2009}$) was expressed as an operon, along with BppA$_{Tuc2009}$ and BppL$_{Tuc2009}$. This construct was generated by SOE, where the BppU-24$_{Tuc2009}$-encoding fragment was amplified using the UAL_F and UΔCt24aa_SOE (*ATTATCCCCCGTTTTCCC*TTACACTTTTTCAACATAGCCT) primer combination. Primers AΔCt24aa_SOE (*GGGAAAACGGGGGATAAT*ATGGCAGATAAAAAT) and UAL_R were used to generate the BppAL$_{Tuc2009}$-specifying region. These two amplicons were mixed to provide the combined template for the SOE PCR with the UAL_F and UAL_R primers to generate the BppU-24AL$_{Tuc2009}$-encoding product, which was cloned into pTX8048. An equivalent construct was generated for the BppUct$_{Tuc2009}$ model. Primers UCt_F and UΔCt24aa_SOE were used to amplify a BppUct-24$_{Tuc2009}$-specifying amplicon, which was mixed with the BppAL$_{Tuc2009}$-encoding amplicon and amplified with UCt_F and UAL_R to yield the BppUct-24AL$_{Tuc2009}$-specifying fragment, which was then cloned into the pTX8049 vector.

Protein expression and purification. Protein expression was based on a system that combines use of the nisin-inducible expression system and thioredoxin fusion (32). Recombinant plasmids containing the regions of interest were transformed into *L. lactis* NZ9000. They were grown overnight at 30°C in GM17 broth supplemented with chloramphenicol at 5 μg/ml. Two percent of this overnight bacterial culture was inoculated into fresh GM17-chloramphenicol and incubated at 30°C. When the optical density at 600 nm (OD_{600}) reached 0.2, protein expression was induced by adding Nisaplin at a concentration of 40 ng/ml. Growth was allowed to continue for another 4 h, at which time the cells were harvested from suspension by centrifugation (8,700 × *g* for 10 min at 4°C). The bacterial pellet was subsequently washed in buffer (10 mM Tris, 300 mM NaCl, 10 mM $CaCl_2$, pH 8) and stored at −20°C.

Bacterial pellets isolated at the protein expression step were defrosted at room temperature, resuspended in buffer (10 mM Tris, 300 mM NaCl, 10 mM $CaCl_2$, pH 8, with 25 mg/ml lysozyme), and incubated for 30 min at 20°C. After incubation, the calcium levels in the sample were supplemented to bring the final $CaCl_2$ level up to 50 mM, and the sample was placed on ice. The samples were then sonicated in an MSE Soniprep (Sanyo, Japan) at 20 μm (maximum amplitude) for 30 s, followed by a minute on ice for 5 cycles. This was followed by centrifugation (25,000 × *g* for 30 min at 4°C) to remove cell debris and insoluble components of the sample. The samples were run on 12.5% SDS-PAGE gels to confirm the presence of induced target proteins, and their identities were confirmed by Western blotting as outlined previously (32) and using polyclonal antibodies raised against BppU$_{Tuc2009}$, BppL$_{Tuc2009}$, or BppA$_{Tuc2009}$ (34).

Purification was based on His-tagged proteins (a His tag present at the C-terminal end of thioredoxin, which in turn was located at the N-terminal part of the target protein) by employing the PrepEase Histidine-tagged Protein Purification kit, utilizing a Ni-Tris(carboxymethyl)ethylene diamine (TED)-based system (USB, USA) or Ni-nitrilotriacetic acid (NTA) agarose (Qiagen, United Kingdom). The protocols for both kits were modified so that the basic buffer in each case was 10 mM Tris, 300 mM NaCl, 50 mM $CaCl_2$, pH 8; imidazole was added to this buffer to mimic the original protocols, as recommended by the manufacturers. Where necessary, protein complexes were further purified on an Äkta fast-performance liquid chromatography system, using a Superose 6 PG XK 16/70 gel filtration column (GE Healthcare, USA), in a buffer constituted of 10 mM Tris, 300 mM NaCl, 50 mM $CaCl_2$, pH 8, at a flow of 1 ml/min. Protein complexes were concentrated using an Amicon Ultra centrifuge device with a 10-kDa mass cutoff (Millipore). The protein concentration of the baseplate complexes was determined by Bradford assay (35).

Production of purified Tuc2009 particles. Tuc2009 phage lysate (3.6 liters) was generated in M17 broth (Oxoid Ltd.) supplemented with 0.5% glucose and 10 mM $CaCl_2$. The lysate was generated using a 2% inoculum of the host strain *Lactococcus lactis* subsp. *cremoris* UC509.9 infected with a fresh, small-scale lysate (35 ml) of a titer of 10^8 PFU/ml. The mixture was incubated at 30°C until lysis was observed. Upon lysis of the culture, sodium chloride was added to a final concentration of 0.5 M and supplemented further with $CaCl_2$ to a final concentration of 50 mM. Bacterial debris was removed by centrifugation at 6,000 rpm for 15 min. To the supernatant, polyethylene glycol 8000 (PEG 8000) was added to a final concentration of 10% (wt/vol) and incubated for 7 h at 4°C, after which the suspension was centrifuged at 9,000 rpm for 20 min. The pellet was subsequently resuspended in a minimal volume of phage buffer (20 mM Tris-HCl, pH 7.5, 10 mM $MgCl_2$, 100 mM NaCl, 50 mM $CaCl_2$). The PEG 8000 was removed by extraction with an equal volume of dichloromethane. The resulting clarified lysate was then applied to a Sephacryl 500 gel filtration system at a flow rate of 2.5 ml/min, and 4-ml fractions were collected in phage buffer (phage eluted at 36 to 52 ml). After filtration through a 0.45-μm filter, the fractions containing phages were concentrated by ultracentrifugation at 22,000 rpm in a Beckman SW41 rotor. The pellets were resuspended in a minimal volume of phage buffer (50 to 100 μl). The resultant phages were of suitable purity for EM analysis.

Electron microscopy. (i) Sample preparation. Three microliters of sample at a final concentration of 0.05 mg/ml was deposited on a glow-discharged carbon-coated copper grid. After 1 min in contact with the carbon film, excess solution was blotted, and 10 μl of 2% uranyl acetate was added to the grid for 1 min. The grid was then air dried and transferred for observation. When nanogold was required, a commercially available nanogold, Ni-NTA-Nanogold (Nanoprobes, USA), was utilized.

(ii) Data collection. Charge-coupled device (CCD) images (baseplate, 2,000; BppUAL$_{Tuc2009}$, 100; and BppUctAL$_{Tuc2009}$, 100) were recorded under low-dose conditions with an FEI Tecnai Spirit microscope operated at 120 kV. Images were recorded at a magnification of ×67,500 (3.53 Å/pixel) for BppUAL$_{Tuc2009}$ and BppUctAL$_{Tuc2009}$ and ×48,500 (4.95 Å/pixel) for the baseplate.

(iii) Image processing. Particles (baseplate, 2,000; BppUAL$_{Tuc2009}$], 5,400; and BppUctAL$_{Tuc2009}$, 5,100) were selected using the program Boxer from the EMAN2 package (36), extracted into boxes of 128 by 128 pixels for the tripods and 144 by 144 pixels for the baseplate, and combined into three different data sets. The data sets were pretreated using the SPIDER package (37) and submitted to maximum-likelihood (ML) classification and alignment (38) using the Xmipp package (39). Initial models were built to form a visually selected class average imposing the corresponding symmetry, C3 for the tripods and C6 for the baseplate. These initial models were then refined by three-dimensional ML refinement. The baseplate was further refined by projection matching with a sampling rate of 5° using SPIDER. After refinements, final models were obtained at resolutions of approximate 44 Å (BppUAL$_{Tuc2009}$), 23 Å (BppUctAL$_{Tuc2009}$), and 36 Å (baseplate), as estimated by Fourier shell correlation (FSC) and the 1/2-bit threshold criterion (reference 40 and data not shown).

(iv) Structure visualization. Molecular graphics and analyses were done with the UCSF Chimera package (41; Resource for Biocomputing, Visualization, and Informatics at the University of California, San Francisco [supported by NIGMS P41-GM103311]). The model-EM map or EM map-EM map fitting was performed by the option "fit in map" of the "volume" register. The difference maps were calculated by the "vop substract" command.

Adsorption assays. Adsorption assays were carried out based on a protocol outlined previously (42). Cells were grown to late exponential phase (OD_{600}, ~0.7). The cells were centrifuged (15,000 × *g*; 3 min) and resuspended in 1/4-strength Ringer's solution. Phages were added to a final concentration of 10^6 PFU/ml. Following incubation at 30°C for 12.5 min, the bacterial host cells were removed by centrifugation. The supernatant was retained, and the remaining phage level was determined by plaque assay.

The tripod-mediated adsorption inhibition assay is an adaptation of the adsorption assay method. Late-exponential-phase lactococcal host

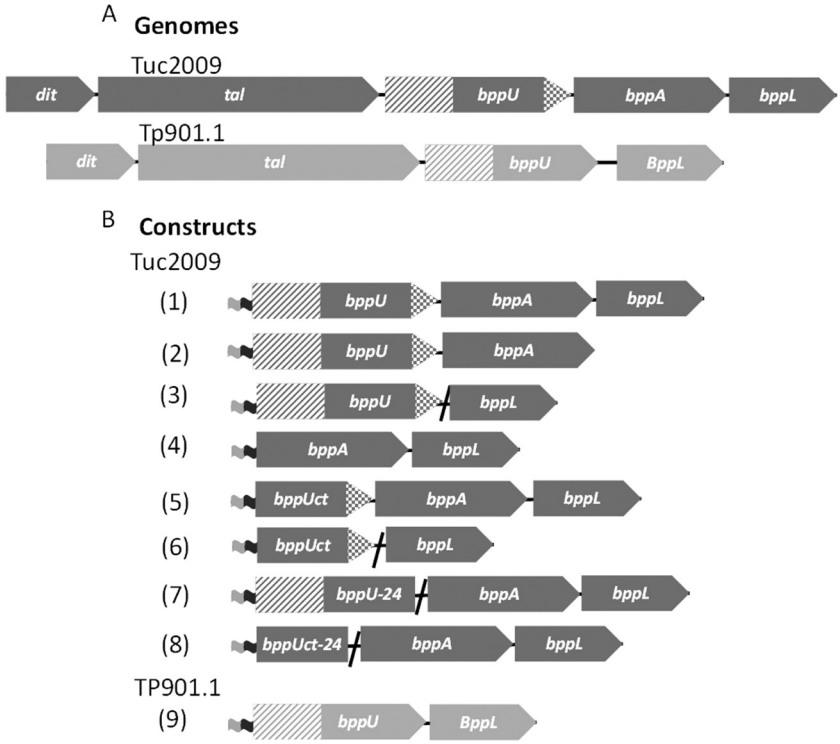

FIG 1 Phage expression constructs. (A) Schematic presentation of the genomic regions of Tuc2009 and TP901-1 encoding the phage baseplate proteins. (B) Schematic representation of constructs for expressing phage protein complexes. The numbers in parentheses correspond to the expression constructs in Table 1. The Tuc2009 *bppU* gene is represented by three different gray patterns: checkered, representing the 24-amino-acid "hanger," and solid gray and hatched gray together, representing the portion of the *bppU* gene that encodes the C-terminal region. The *bppU* section encoding the N-terminal portion is indicated by hatched gray. For TP901-1, the DNA encoding the BppU N-terminal region is hatched, while that specifying the C-terminal portion is indicated in solid gray. The light-gray and black flags represent DNA regions to facilitate thioredoxin and His_6 tag fusions, respectively.

cells (225 μl) resuspended in Ringer's solution were added to a tube to which either 50 μl of buffer (negative control) or tripod complex was added. This cell-tripod mixture was incubated at 30°C for 1 h, and at this stage, phage were added to give a PFU count of 10^6 per ml and a total reaction volume of 0.5 ml. This mixture was incubated at 30°C for 12.5 min, host cells were removed by centrifugation, the supernatant was retained, and the remaining PFU were determined using the double-agar method (43).

Accession numbers. The EM structures of Tuc2009 $BppUAL_{Tuc2009}$ and BppU-$CtAL_{Tuc2009}$ tripods and of the Tuc2009 baseplate were deposited at the Electron Microscopy Data Bank (EMDB) under the accession numbers EMD-2345, EMD-2343, and EMD-2340, respectively.

RESULTS

Cloning and production of Tuc2009 phage proteins. Tuc2009 belongs to the P335 species of lactococcal phages and possesses a baseplate composed of a hetero-oligomeric protein complex (30). The structural genes encoding the baseplate are found in the Tuc2009 genomic region, which starts at the distal tail gene (*dit*) and ends with the *bppL* gene (Fig. 1A). Analogous to the situation in TP901-1, it was expected that the Tuc2009 baseplate contains six so-called tripods, each of which exists as a $BppU_{Tuc2009}$-$BppA_{Tuc2009}$-$BppL_{Tuc2009}$ protein complex ($BppUAL_{Tuc2009}$), which had until now been recalcitrant to advanced structural characterization (16). In order to achieve maximal protein (complex) production of the Tuc2009 tripod or parts thereof, we performed protein expression in *L. lactis* NZ9000. A recently developed lactococcal expression vector that incorporates the inducible NICE system and thioredoxin gene fusion (32) was successfully employed for this study, allowing soluble and stable (co)production of various Tuc2009 tripod proteins at a high yield (the various cloned and expressed genes are schematically outlined in Fig. 1B). This approach utilized an operon-based *E. coli*-based cloning and expression strategy previously described for the characterization of TP901-1 and p2 phage baseplates (16).

In this way, we achieved coexpression of a number of Tuc2009 tripod protein complexes (Fig. 1 and 2), representing the following protein combinations: $BppU_{Tuc2009}$-$BppA_{Tuc2009}$ ($BppUA_{Tuc2009}$), $BppU_{Tuc2009}$-$BppL_{Tuc2009}$ ($BppUL_{Tuc2009}$), $BppA_{Tuc2009}$-$BppL_{Tuc2009}$ ($BppAL_{Tuc2009}$), and $BppUAL_{Tuc2009}$. All constructs were generated using the lactococcal expression vectors pTX8048 and pTX8049, allowing the first protein encoded by the constructed operon to become translationally fused at its N terminus to a thioredoxin and hexahistidine (His_6) tag. When the His_6-tagged protein is purified, the second and, for some constructs, third protein products encoded by the operon are copurified if they form protein complexes with this His_6-tagged product, as was shown previously for other baseplate-tripod complexes (16). Production of all protein combinations was successful, with a relatively high yield of between 1 and 4 mg/liter (Fig. 2A), except for the $BppAL_{Tuc2009}$ pairing, which produced negligible amounts of protein (data not shown). The generation of a $BppUAL_{Tuc2009}$ complex had previously been attempted in *E. coli* without much success (16) yet was successful when *L. lactis* was used as the expression host

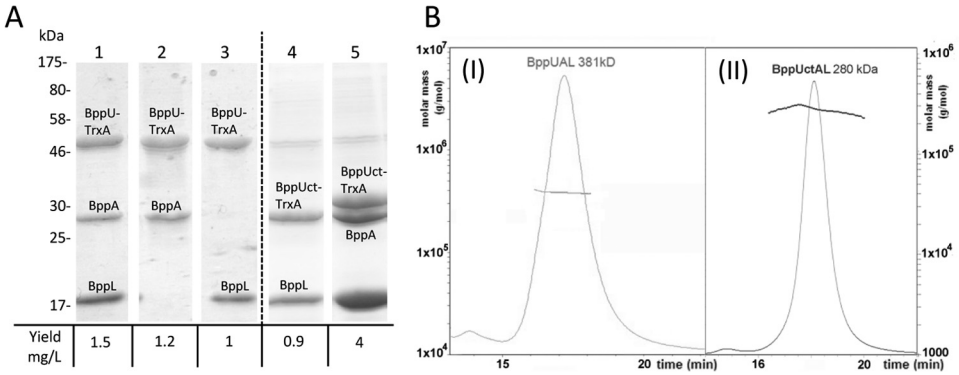

FIG 2 Production and analysis of Tuc2009 tripod protein complexes. (A) SDS-PAGE analysis of the His-tagged purified protein products expressed by *L. lactis* NZ9000 cells harboring pTX8048-UAL (lane 1), pTX8048-UA (lane 2), pTX8048-UL (lane 3), pTX8049-BppUctL (lane 4), and pTX8049U-CtAL (lane 5). The Tuc2009 tripod protein products are indicated in the text. (B) SEC-MALS-RI analysis of the tripod complexes. The molar mass (left axis; solid lines) and the UV_{280} absorbance (right axis; dashed lines) are plotted as functions of the column elution volume. (I) BppUAL. (II) Tuc2009 BppUctAL complex.

(32), while we further improved the induction and extraction procedure to allow production of this protein complex at levels suitable for further characterization (Fig. 2A). In addition, we successfully purified $BppUA_{Tuc2009}$ and $BppUL_{Tuc2009}$ complexes, demonstrating that $BppU_{Tuc2009}$ on its own acts as the binding partner of either $BppL_{Tuc2009}$ or $BppA_{Tuc2009}$, despite the absence of the third protein component of the Tuc2009 tripod (Fig. 2A).

The structure of the Tuc2009 tripod complex. The tripod complex of phage Tuc2009 is composed of open reading frames (ORFs) similar to those of TP901-1, with the exception of BppA, which is not encoded by TP901-1 (Fig. 1A). The BppU proteins of Tuc2009 and TP901-1 exhibit high identity (97%) within the first 180 residues; however, their C termini are more divergent (52% identity). Furthermore, $BppU_{Tuc2009}$ possesses a 24-residue C-terminal extension relative to $BppU_{TP901-1}$ (Fig. 3A). $BppL_{Tuc2009}$ and $BppL_{TP901-1}$, which represent the RBPs of Tuc2009 and TP901-1, respectively, are the most divergent proteins among the baseplate components of the two phages: some identity is present within the first 60 residues, in particular amino acid residues 9 to 20 and 38 to 50 ($BppL_{TP901-1}$ numbering) (data not shown). Beyond residue 60, the two proteins lack sequence similarity, which is assumed to be responsible for the distinct receptor binding specificity of each of these RBPs and explains the specific host ranges exhibited by their corresponding phages. The successful expression of Tuc2009 proteins allowed us to further characterize the Tuc2009 tripod, which was purified as a $BppUAL_{Tuc2009}$ complex of 381 kDa, as determined by size-exclusion chromatography–multiangle light-scattering–refractive index (SEC-MALS-RI) analysis (Fig. 2B, I). This molecular mass of the hetero-oligomeric protein complex is consistent with a stoichiometry of 3 $BppU_{Tuc2009}$, 2 $BppA_{Tuc2009}$, and 9 $BppL_{Tuc2009}$, which has a theoretical mass of 388 kDa.

The Tuc2009 tripod complex was shown to exhibit a well-defined structure by single-particle EM reconstruction, consistent with findings for the related phage TP901-1 (15) (Fig. 4A). However, whereas the three RBP trimers fit exactly within this tripod, the "upper part" of the EM density was more difficult to assign, possibly due to the disorder of the large $BppU_{Tuc2009}$ N-terminal domains. In order to simplify the assignment, we expressed a complex of $BppUct_{Tuc2009}$, encompassing only the C-terminal portion of $BppU_{Tuc2009}$ (corresponding to residues 194 to 322, similar to what has been described for $BppU_{TP901-1}$ (18) (Fig. 1). Interestingly, this complex was shown by MALS-RI to exhibit a mass of 290 kDa, accounting for a stoichiometry of 3 $BppUct_{Tuc2009}$, 3 $BppA_{Tuc2009}$, and 9 $BppL_{Tuc2009}$ (theoretical mass, 306 kDa) (Fig. 2A and B, II), demonstrating that the removal of the N-terminal portion (residues 1 to 193) of $BppU_{Tuc2009}$ does not impact the truncated protein's ability to complex with $BppA_{Tuc2009}$ and $BppL_{Tuc2009}$ while, surprisingly, allowing the inclusion of an additional $BppA_{Tuc2009}$ protein in the resulting tripod. This complex was readily assigned in the EM maps by fitting the molecular structure of its counterpart from TP901-1 (BppU C terminus and BppL), which was solved by X-ray crystallography (29) (Fig. 4D). Upon subtraction of the X-ray map of the BppUct tripod of TP901-1 from the EM map of the Tuc2009-corresponding BppUct tripod, we obtained a globular difference map accounting for three $BppA_{Tuc2009}$ proteins located on top of the tripod and interacting laterally with BppUct (Fig. 4F). Mass calculations of this differential volume were performed, which yielded, assuming a density of 1.44 Da/Å^3, a calculated mass of 300 kDa versus a theoretical mass of 306 kDa.

The baseplate structure. Detailed analysis of the complete Tuc2009 baseplate was also carried out. Based on previous work (30), we assumed that the phage Tuc2009 baseplate is composed of an oligoheteromeric complex of five different proteins: ORF49 ($Dit_{Tuc2009}$), ORF50 (Tal_{2009}), ORF51 ($BppU_{Tuc2009}$), ORF52 ($BppA_{Tuc2009}$), and ORF53 ($BppL_{Tuc2009}$). Single-particle electron microscopy was used to examine the baseplate region of Tuc2009 phage particles, a technique that has previously proven to be very powerful for other lactococcal-phage baseplates, such as those of phage p2 (16) and TP901-1 (15, 29). For the purpose of this experiment, we collected ~2,000 EM images of phage Tuc2009 using negative staining. We boxed images of the Tuc2009 phage around the baseplate, including a small part of the tail, and performed single-particle EM reconstruction with 6-fold symmetry averaging (see Materials and Methods for further details). The observed overall EM density resembles that obtained for the baseplate phage of TP901-1, in agreement with the very high sequence identity of the individual protein components that form their baseplates. The Tuc2009 baseplate displays a 6-fold-symmetry structure with dimensions corresponding to 290-Å diameter and 160-Å height (Fig. 5). The EM density of the Tuc2009 tripod structure (Fig. 4) can be fitted readily in one of the sextants of the

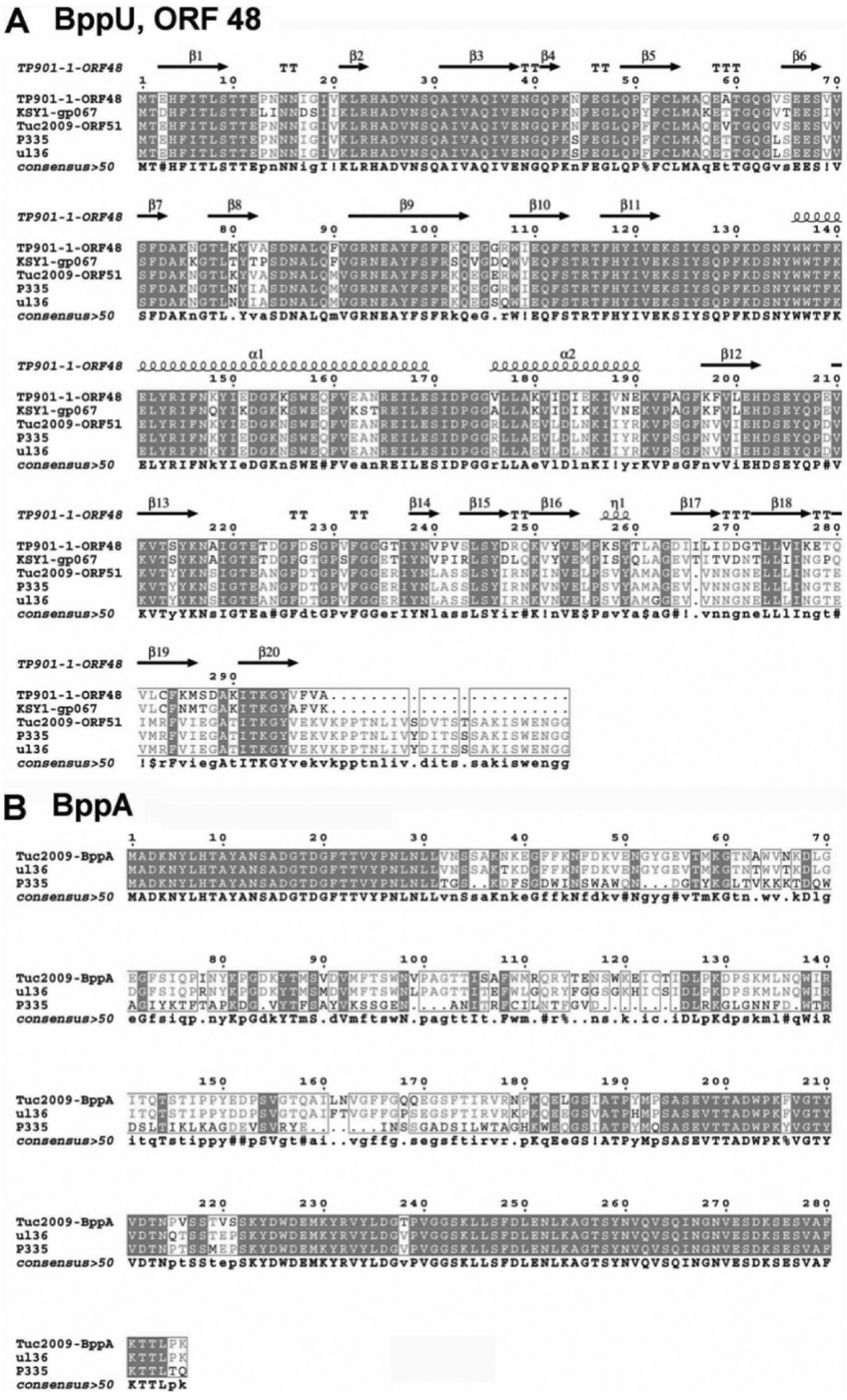

FIG 3 Sequence alignment of upper and accessory baseplate proteins. (A) Amino acid alignment of BppU protein homologues from TP901-1, Tuc2009, KSY1, P335, and UL36. The secondary structure is indicated above the alignment. (B) Amino acid alignment of BppA protein homologues from Tuc2009, UL36, and P335. For both alignments, regions of identity are highlighted in gray, and consensus is shown below the alignment. Uppercase signifies identity, lowercase is a consensus level of >0.5, ● is unconserved, $ is L or M, % is F or Y, ! is I or V, # can be one of DENQ, and * is one of EVADK.

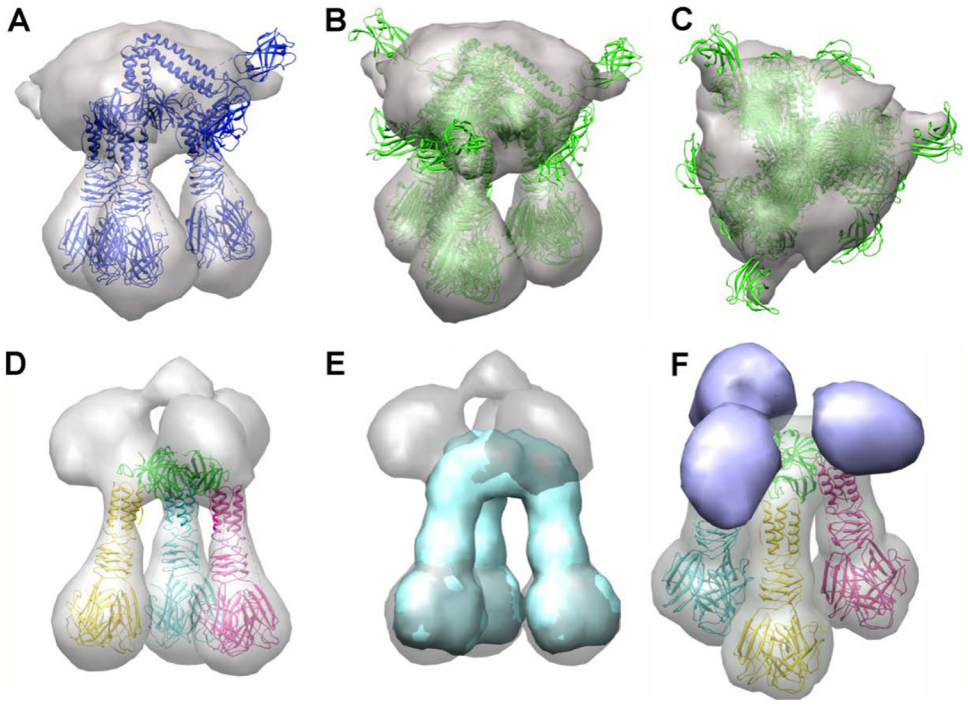

FIG 4 EM map of Tuc2009 tripod. (A to C) The BppU (full length), BppA, and BppL complex. In panel A, only a tripod is displayed, while in panels B and C, the three possible orientations are shown. The EM map appears as a gray transparent surface. (D to F) The BppUct, BppA, and BppL complex. (D) The TP901-1 X-ray-determined BppUct-BppL complex fitted into the EM map (gray). (E) The blue surface corresponds to the 20-Å calculated map of the TP901-1 BppUctBppL complex shown in panel D. (F) The violet blobs result from a calculated difference map between the two maps presented in panel E. The artifact at the top of the density has been removed. These blobs represent three molecules of $BppA_{Tuc2009}$.

baseplate (Fig. 5A). The X-ray structure of the baseplate of phage TP901-1, comprised of $Dit_{TP901-1}$, $BppU_{TP901-1}$, and $BppL_{TP901-1}$, was fitted into the Tuc2009 EM density map using Chimera (41). The position of each $BppL_{TP901-1}$ trimer was then optimized into each of the $BppL_{Tuc2009}$ trimer densities, and the Dit-$BppU_{TP901-1}$ complex was optimized as a whole in the corresponding density of the Tuc2009 baseplate. The results show a remarkable fit of the complete TP901-1 baseplate into the Tuc2009 EM density map (Fig. 5B to D). We then subtracted the electron density of the molecular model, calculated at 20 Å, from the experimental EM density of the Tuc2009 baseplate (Fig. 6A, B, and C). This resulted in a small number of residual densities in the raw difference map, corresponding to the virion's tail (Fig. 6B and C, top), the Tal_{2009} trimer (Fig. 6C, bottom), and $BppA_{Tuc2009}$ (Fig. 6A and B, equatorial position). The various components of this differential map (Fig. 6C, D, and E) were then separated and "cleaned," and only the first ring of the tail was retained, thereby erasing the rest of the density. The structures of the major tail protein (MTP) (Fig. 6D to F, orange) appear quite clear, with its ~40-Å-diameter channel inside, and are in contact with $Dit_{Tuc2009}$ (Fig. 6E and F, bottom), which exhibits a channel of the same size. The tail fiber of Tuc2009, called the tail-associated lysin (Tal_{2009}) (44, 45) (Fig. 6D to F, blue), appears as a 6-fold-symmetry structure, in spite of being a trimer (30), because two structures can superimpose with a 60° rotation (and not 120°), leading to pseudo-6-fold symmetry. However, the general size and the contacts between Tal_{2009} and the rest of the baseplate are in agreement with expectations. Tal_{2009} is in contact with the N terminus of $Dit_{Tuc2009}$, which forms a ring with a 40-Å internal channel (Fig. 6G). Tal_{2009} also contacts the inner $BppL_{Tuc2009}$ trimers. The other face of the ring is in contact with the first MTP ring (Fig. 5G). Finally, $BppA_{Tuc2009}$ appears as two elongated density bulbs (Fig. 6D and G), rather than three, attached to the $BppU_{Tuc2009}$ C terminus. As outlined in Fig. 6D, the two elliptical densities (red) are positioned against two faces of the triangular $BppU_{Tuc2009}$ (blue). The third face of the BppU C terminus cannot accommodate a third $BppA_{Tuc2009}$ (as in the $BppUctAL_{Tuc2009}$ tripod [see above]), because the position (black ellipsoid) is occupied by the elongated three-helix bundle, which connects the N-terminus trimeric ring of $BppU_{Tuc2009}$ to its C terminus, as observed in the phage TP901-1 baseplate (29).

$BppA_{Tuc2009}$ requires the $BppU_{Tuc2009}$ C-terminal extension for complex formation. When the baseplates of Tuc2009 and TP901-1 are contrasted, a key difference between them is the presence of the $BppA_{Tuc2009}$ protein in the Tuc2009 baseplate (see above). It was noted that a 24-amino-acid region is present in the C-terminal region of the Tuc2009 BppU protein, whereas TP901-1, which does not encode a BppA protein, lacks this C-terminal extension in its BppU primary sequence. This 24-amino-acid region is also present in other BppU homologues encoded by various phages, such as P335 and ul36 (Fig. 3), which do encode a BppA protein. It was therefore hypothesized that this 24-aa extension is required to attach BppA to the baseplate, thus acting as a "hanger" for BppA. In order to test this, we generated two constructs, pTX8048U-24AL and pTX8049Uct-24AL, in which $BppU_{Tuc2009}$ and $BppUct_{Tuc2009}$ are expressed as proteins carrying a 24-amino-acid C-terminal truncation (designated BppU-$24_{Tuc2009}$ and BppUct-$24_{Tuc2009}$), respectively, alongside the $BppA_{Tuc2009}$ and $BppL_{Tuc2009}$ proteins (Fig. 1). The (co)expressed

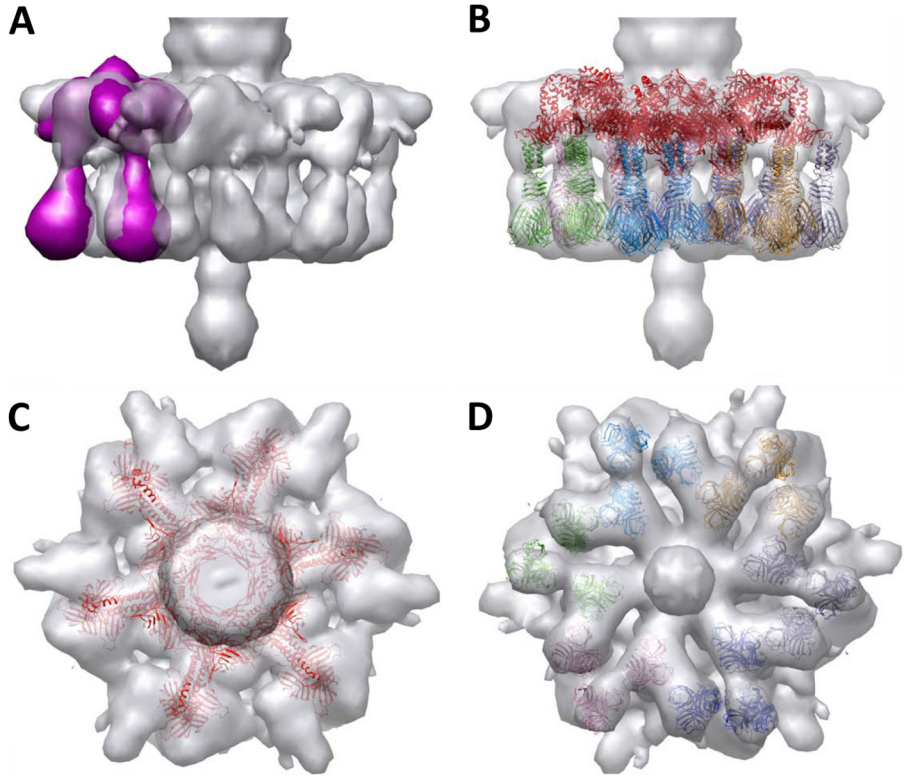

FIG 5 Negatively stained EM map of Tuc2009 baseplate. (A) The tripod ($BppUctAL_{Tuc2009}$) EM map (violet) fitted into the EM map of the baseplate of phage Tuc2009 (gray). (B) The molecular X-ray structure of the baseplate of TP901-1 fitted into the EM map of the baseplate of phage Tuc2009. The fit of each BppL trimer was optimized locally. The three BppL trimers that form the "legs" of a given tripod are depicted in a specific color, with legs of different tripods in distinct colors. BppU (top) is colored red. (C) View from the top. (D) View from the bottom.

products of these constructs were then assessed, in particular, the presence or absence of the $BppA_{Tuc2009}$ protein in the crude lysate and in the His-tagged purified protein products by SDS-PAGE analysis. Upon induction of these tricistronic vectors, a protein band representing $BppL_{Tuc2009}$ was clearly observed by SDS-PAGE in the soluble fractions (Fig. 7A). Although $BppA_{Tuc2009}$ is not visible in the crude cell extract, as is typical for this type of polycistronic induction in *L. lactis*, the protein is nevertheless ex-

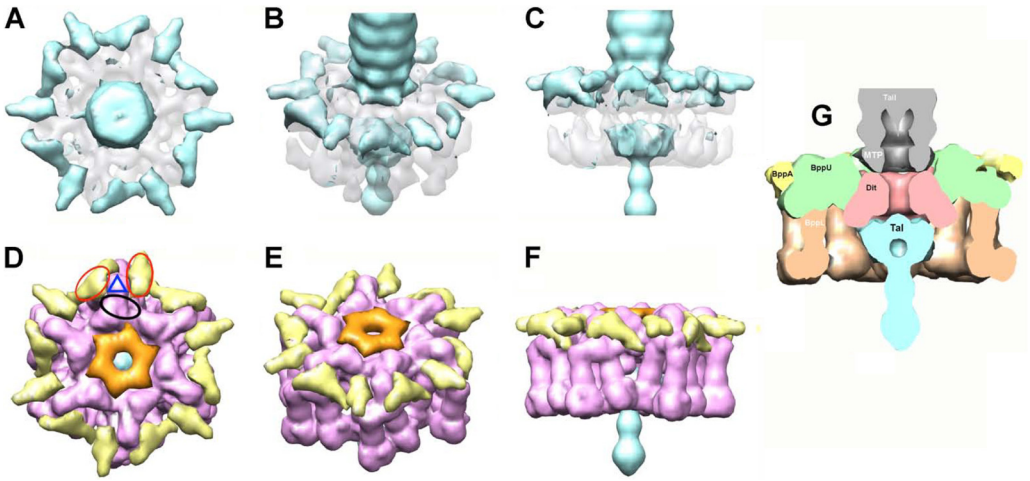

FIG 6 EM map analysis and molecular assignment of Tuc2009 baseplate. (A to C) A difference map (blue) was obtained by subtracting the 20-Å-resolution calculated map of the X-ray structure of the baseplate of TP901-1 from the EM map of the baseplate of phage Tuc2009 (gray). Three areas of difference density are observed in the tail (top), BppA (periphery), and the Tal trimer (bottom). (A) Top view. (B) 45° view. (C) Lateral view. (D to F) The difference map was smoothed and assigned different colors: the first tail ring is orange, BppA is yellow, and Tal is indicated in blue. The 20-Å-resolution calculated map of the X-ray structure of the baseplate of TP901-1 is pink/purple. (D) Top view. (E) 45° view. (F) Lateral view. The C-terminal domain of BppU is schematically indicated as a triangle, while the two BppA blobs are depicted as red ellipsoids. The dark ellipsoid covers the position of the BppU helices, which prevents binding of a third BppA. (G) The same EM maps are displayed, but a different EM map was calculated for Dit (pink), BppU (green), and BppL (brown). The tail is gray, and BppA is indicated in yellow.

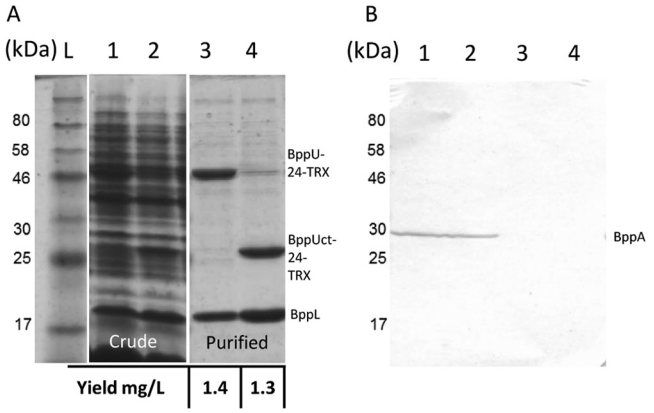

FIG 7 BppU C-terminal deletion. (A) Protein gel analysis of the crude soluble fractions of induced NZ9000 plus pTX8048U-24AL (lane 1) and NZ9000 plus pTX8049Uct-24AL (lane 2) and of purified fraction from induced NZ9000 plus pTX8048U-24AL (lane3) and NZ9000 plus pTX8049Uct-24AL (lane 4). Lane L contains a prestained protein marker. (B) Immunoblot analysis showing BppA, using anti-BppA rabbit polyclonal antibody as a primary antibody. Shown are crude soluble fractions of induced NZ9000 plus pTX8048U-24AL (lane 1) and NZ9000 plus pTX8049Uct-24AL (lane 2) and purified fraction from induced NZ9000 plus pTX8048U-24AL (lane 3) and NZ9000 plus pTX8049Uct-24AL (lane 4).

pressed, as shown by Western blotting (Fig. 7B, lanes 1 and 2). When Tuc2009 tripod proteins are expressed as full-length proteins, it is possible to simultaneously purify all three proteins as a complex, based on a His_6 tag at the N terminus of $BppU_{Tuc2009}$, due to their inherent affinity for $BppU_{Tuc2009}$ (Fig. 2A) (32). However, when we carried out a nickel affinity purification of BppU-$24_{Tuc2009}$ or BppUct-$24_{Tuc2009}$, only these His_6-tagged proteins and $BppL_{Tuc2009}$ were purified, while $BppA_{Tuc2009}$ was not detectible, even by Western blotting (Fig. 7A and B, lanes 3 and 4), based on which we conclude that the 24-aa C-terminal region of $BppU_{Tuc2009}$ is required for the attachment of $BppA_{Tuc2009}$ to $BppU_{Tuc2009}$.

EM analysis of tripod binding. The tripods of Tuc2009 and TP901-1 contain the BppL/RBP protein, which is believed to specifically interact with receptors at the bacterial surface. To assess if recombinantly produced tripods can indeed interact specifically with their bacterial host, immunogold electron microscopy of *L. lactis* UC509.9 incubated with 3 μM Tuc2009 tripod ($BppUAL_{Tuc2009}$) or *L. lactis* 3107 incubated with a similar amount of the TP901-1 tripod ($BppUL_{TP901-1}$; expressed as outlined in Fig. 1) was carried out using nanogold particles that possess a His_6-binding tag. Since gold labeling is expected to occur only with molecules bearing a His_6 tag, i.e., the tripods, this experiment permitted an assessment of the specificity and localization of tripod-host receptor binding. The immunogold electron micrographs showed that the tripods were localized uniformly on the host cell surface, indicating that the host receptor molecules are evenly distributed around the cell (Fig. 8A), a finding that is consistent with the saccharidic nature of the proposed receptor for these phages. A high degree of specificity was demonstrated based on the incubation of TP901-1 tripods with *L. lactis* UC509.9 host cells, where negligible binding was noted (Fig. 8C). These findings are replicated if *L. lactis* 3107 is used as the host strain.

Tripod adsorption inhibition assays. Based on the observation that the $BppUAL_{Tuc2009}$ protein complex adopts a tripod conformation that fits into the EM model of the Tuc2009 baseplate, combined with the immunogold EM data showing that Tuc2009 tripods bind specifically to their host cells, it was decided to establish if these recombinantly produced tripods could act as competitors for phage adsorption. For this purpose, we incubated late-exponential-phase cells of the Tuc2009 host, *L. lactis* UC509.9, with increasing concentrations of Tuc2009 tripod complex. Following an incubation period, 10^6 PFU of Tuc2009 phage was

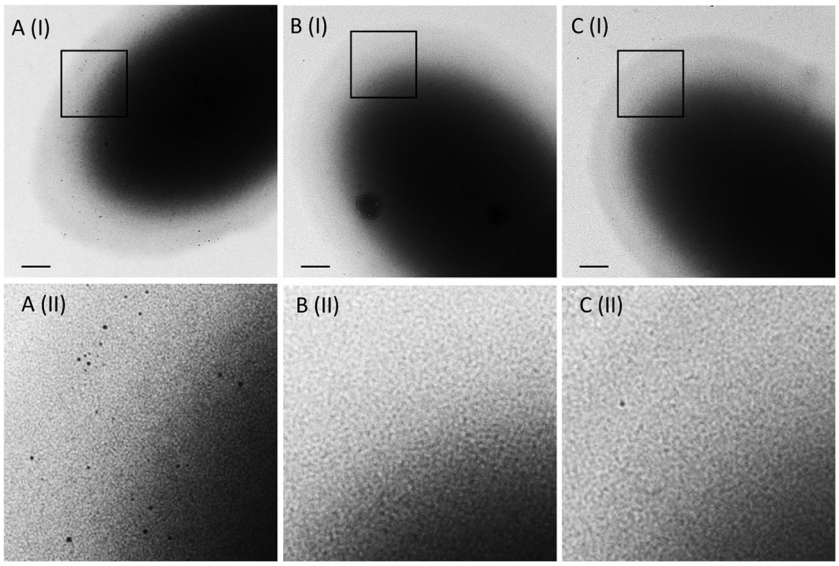

FIG 8 Immunogold labeling of tripods attached to cells. (A) *L. lactis* UC509.9 incubated with Tuc2009 tripods, followed by immunogold EM analysis. The black dots on the image represent gold particles bound to the His_6 tag present on the BppU component of the tripod. (B) Buffer incubation. Shown is *L. lactis* UC509.9 incubated with buffer, followed by labeling with immunogold. (C) Negative control. Shown is *L. lactis* UC509.9 incubated with TP901-1 tripods, followed by labeling with immunogold. (I) Partial cell images. (II) Zoom image corresponding to the boxed areas.

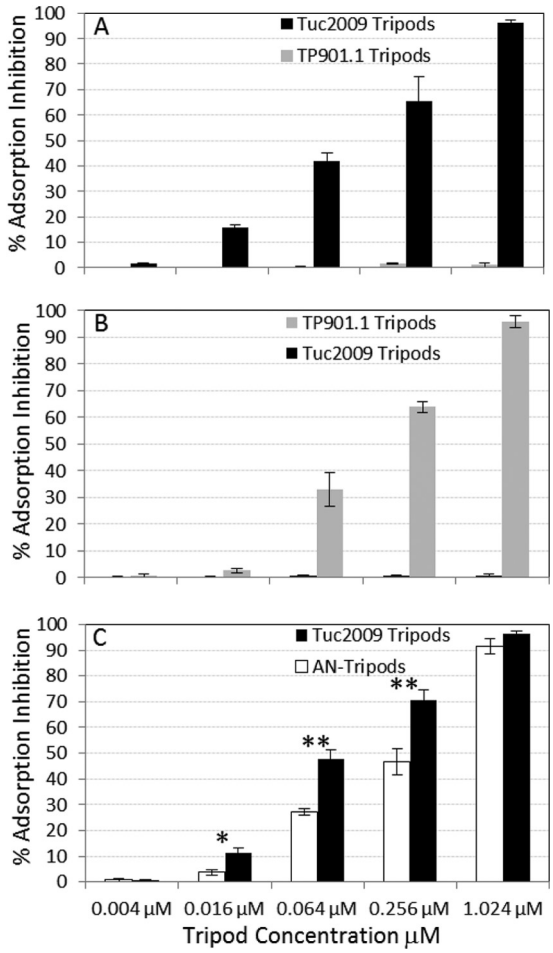

FIG 9 Adsorption-blocking assays. (A) Adsorption inhibition was determined when *L. lactis* UC509.9 was incubated with increasing levels of either Tuc2009 or TP901-1 phage tripods, followed by adsorption assays using Tuc2009. (B) *L. lactis* 3107 was incubated with increasing levels of either Tuc2009 or TP901-1 phage tripods, followed by adsorption assays using TP901-1. (C) *L. lactis* UC509.9 was incubated with increasing levels of either AN tripods or Tuc2009 tripods, followed by adsorption assays using Tuc2009. The error bars represent the standard deviations of three independent experiments performed in triplicate. *, $P < 0.05$; **, $P < 0.01$.

added to the mixture, after which Tuc2009 adsorption was measured. Remarkably, incubating bacterial cells with Tuc2009 tripods was shown to result in a reduction of Tuc2009 adsorption to the host cell, a phenomenon here termed adsorption inhibition (the measure of adsorption reduction in the presence of tripods compared to the adsorption in the negative control [buffer only]). The adsorption inhibition effect was dose dependent and was seen across a range of concentrations (Fig. 9). At a tripod concentration of 1.024 μM, adsorption inhibition of 96% was achieved, while a pronounced effect was observed even at a lower tripod level of just 0.016 μM, providing 15% inhibition (Fig. 9A). We further sought to investigate if this protective effect was limited to Tuc2009 tripods or if it was possible to replicate the effect using an alternative tripod-host-phage combination. To that end, TP901-1 tripods were incubated with *L. lactis* 3107 cells and challenged with TP901-1 phage, and a similar phenomenon was observed; a low level of adsorption inhibition of 2.6% was noted at 0.016 μM, and as the TP901-1 tripod concentration was increased, adsorption inhibition gradually rose to 95% (at a TP901-1 tripod concentration of 1.024 μM) (Fig. 9B). Adsorption inhibition assays were also performed in which lactococcal cells were incubated with a noncorresponding tripod, i.e., UC509.9 (Tuc2009 host) with TP901-1 tripod and 3107 (TP901-1 host) with Tuc2009 tripod. The results obtained, as displayed in Fig. 9A and B, clearly show that essentially no adsorption inhibition was provided by tripods from a noncorresponding phage; even at the highest tested concentration of tripods, the percentage of adsorption inhibition did not exceed 2%.

The role of BppA in phage adsorption. Since we demonstrated that Tuc2009 tripods, composed of $BppUAL_{Tuc2009}$, can provide adsorption inhibition, presumably by competitive receptor binding, we wanted to investigate the role or contribution of $BppA_{Tuc2009}$ in this phenomenon. For this purpose, we produced Tuc2009 tripods that lack the $BppA_{Tuc2009}$ protein component by making use of the finding that the C-terminal extension of $BppU_{Tuc2009}$ is required for $BppA_{Tuc2009}$ incorporation in the tripod (Fig. 1 and 7) (see Materials and Methods). These BppA-negative tripods (AN tripods) were then used in an adsorption inhibition test, as outlined above, by incubating late-exponential-phase cells of the lactococcal host UC509.9 with increasing levels of tripod complex, followed by the addition of Tuc2009 to the mixture, after which the impact on phage adsorption was measured. The results obtained clearly demonstrate that the AN tripods still confer adsorption inhibition of Tuc2009, ranging from a low level of inhibition of less 3.7% at a tripod concentration of 0.016 μM to a high level of 91.5% at 1.024 μM. The adsorption inhibition assays with AN tripods were carried out in parallel with assays using $BppUAL_{Tuc2009}$ tripods, and when the results obtained are compared, it is noteworthy that the level of adsorption inhibition achieved for the AN tripods is significantly reduced at tripod concentrations of 0.016 μM ($P < 0.05$) and 0.064 and 0.256 μM ($P < 0.01$) concentrations, with approximately 20% less adsorption inhibition noted for AN tripods at the last two concentrations than for $BppUAL_{Tuc2009}$ tripods (Fig. 9C).

DISCUSSION

While there has been much success in the production, characterization, and purification of TP901-1 proteins, the proteins of its relative, phage Tuc2009, have thus far proven resistant to expression and downstream applications, preventing further characterization (16). Here, a combination of optimization approaches was applied to overcome these hurdles and yield sufficient amounts of Tuc2009 protein complexes for further study. We succeeded in further characterizing this model P335 phage and drawing comparisons with its close relative, TP901-1.

We determined the low-resolution structure of the Tuc2009 tripod ($BppUAL_{Tuc2009}$) and baseplate by EM at 20-Å resolution. When we compared the baseplate of Tuc2009 with that of TP901-1, whose structure has been determined (29), they were shown to both possess 6-fold symmetry and to be composed of Dit, Tal, BppU, and BppL, while the Tuc2009 baseplate has an extra protein component, $BppA_{Tuc2009}$, associated with its tripods. The EM difference map made it possible to localize $BppA_{Tuc2009}$ within the $BppUctAL_{Tuc2009}$ tripod, where 3 $BppA_{Tuc2009}$ molecules are bound to the $BppUct_{Tuc2009}$ trimer. However, in the $BppUAL_{Tuc009}$ tripod or in the Tuc2009 baseplate, only 2 $BppA_{Tuc2009}$ molecules are associated per tripod, since the third position is occupied by the $BppU_{Tuc2009}$ horizontal three-helix

bundle that joins the $BppU_{Tuc2009}$ N-terminal domain to the $BppU_{Tuc2009}$ C-terminal domain (29). Therefore, from these data and excluding Tal, we conclude that the Tuc2009 baseplate is a protein complex composed of 6 $Dit_{Tuc2009}$, 18 $BppU_{Tuc2009}$, 12 $BppA_{Tuc2009}$, and 54 $BppL_{Tuc2009}$, which accounts for an overall mass of ~2.2 MDa versus 1.8 MDa for TP901-1. The presence of $BppA_{Tuc2009}$ on the upper region of the tripod may help to stabilize the interaction with $BppL_{Tuc2009}$ (the RBP), since $BppUct_{Tuc2009}$ binds to the RBP trimer. The 24-aa "hanger motif" present in the C-terminal domain of Tuc2009 $BppU_{Tuc2009}$ was shown to be required for the association of $BppA_{Tuc2009}$ to the Tuc2009 tripod structure (Fig. 7). Members of the P335 phage species that encode BppUL baseplate components can be divided into two groups, based on the presence or absence of BppA and the hanger motif (Fig. 3).

Intriguingly, the lactococcal *Podoviridae* phage KSY1 (46) encodes baseplate proteins that are clearly homologous to those found among the P335 species (which belongs to the *Siphoviridae*), particularly those that belong to the TP901-1 group, as its BppU, too, lacks the hanger motif and does not encode BppA either (Fig. 3). The presence of this structure on a nonsiphophage indicates that this carbohydrate recognition device is in operation across a wider range of viruses than is currently appreciated.

The phage tripods discussed here represent the antireceptor units of Tuc2009 and TP901-1 and are required for adsorption to their respective hosts. It is presumed that these units have the capability to specifically bind the host cell through receptors located on the cell surface. Using electron microscopy and immunogold labeling, we were able to observe the interaction of phage tripod units with the cell surface (Fig. 8). In addition, we documented the ability of tripods to inhibit corresponding phage from adsorbing to the host, with adsorption being the prerequisite for infection. To the best of our knowledge, such findings have previously been shown only for recombinantly produced phage antireceptors of the *Podoviridae* and *Siphoviridae* (7, 47). However, the current work describes the first example of an elaborate heteromultimeric antireceptor that is believed to recognize a carbohydrate moiety, as opposed to a specific proteinaceous receptor. The tripod complexes can cause nearly complete phage adsorption inhibition at a concentration as low as 1 μM and still retain measurable activity at 0.016 μM (Fig. 9A). This level of adsorption inhibition is similar to that provided by the pb5 protein of *E. coli* phage T5 (7). For both of the lactococcal tripods described here and pb5, protection is seen in the micromolar range; however, Tuc2009 and TP901-1 tripods appear to have greater efficacy, causing 95% adsorption inhibition at 1 μM. Adsorption inhibition assays were also carried out with tripods lacking $BppA_{Tuc2009}$, showing that $BppA_{Tuc2009}$ is not an essential component for functional tripod binding but that it enhances the adsorption inhibition ability of the Tuc2009 tripod (Fig. 8C). We can therefore view $BppA_{Tuc2009}$ as an accessory protein in the baseplate of Tuc2009 that functions to increase adsorption effectiveness. This role is probably conserved across bacteriophages with baseplates that incorporate a BppA homologue.

It is possible to further quantify the interactions between phage and tripods in our experimental setup, based on an estimation of the surface area required for tripod binding and the surface area of a host cell. If we consider that the pellicle layer covers the entire cell surface area and regard this as a uniformly and ubiquitously present surface receptor, we can estimate that approximately 5×10^4 tripods are required to fully cover the surface of a host cell (note that if this calculation is made based on the surface area of a circle with the diameter of a Tuc2009/TP901-1 baseplate, we can fit approximately 5×10^3 baseplates per cell). When we calculate the number of tripods present per cell in our adsorption assays, they range from 6×10^5 at 1 μM to 2.3×10^3 at 0.004 μM per cell. It follows, then, that at the higher concentration there is an excess of tripods over the number needed to cover the full cell surface area, thus possibly coating the pellicle in a manner that competitively excludes phage from adsorbing to the cell. At 0.004 μM, insufficient tripods are present to fully bind to and competitively exclude phage from all available receptors, therefore hardly impacting phage adsorption.

While the tripods of Tuc2009 and TP901-1 are morphologically similar, we found that their associated adsorption inhibition abilities are specific to their native hosts and corresponding phages (Fig. 9). Crossing the tripods with the alternative hosts yielded no protective effect, accentuating the specificity of these phage tripods and confounding the knowledge that this specificity is exclusively linked to the C-terminal region of BppL and not just a trait associated with the general morphology (Fig. 9).

This study represents the first functional analysis of the baseplate and tripod proteins as a crucial device for saccharide-recognizing phages. Furthermore, while it is established that the block cloning strategy and affinity purification system is useful in terms of the expression and purification of protein complexes, this study provides compelling evidence that these complexes are associated in the correct stoichiometric proportions and are biologically active. While this study relates to the lactococcal P335 phage species, the concept and mechanistic insights may be applied to any tailed phage with affinity for cell surface carbohydrates.

ACKNOWLEDGMENTS

This work has been funded in the Cambillau laboratory by a grant from the Agence Nationale de la Recherche (Lactophages, ANR-11-BSV8-004-01). D.V.S. is the recipient of a Science Foundation Ireland (SFI) Principal Investigator award (no. 08/IN.1/B1909).

REFERENCES

1. **Plisson C, White HE, Auzat I, Zafarani A, Sao-Jose C, Lhuillier S, Tavares P, Orlova EV.** 2007. Structure of bacteriophage SPP1 tail reveals trigger for DNA ejection. EMBO J. **26:**3720–3728.
2. **Valyasevi R, Sandine WE, Geller BL.** 1991. A membrane protein is required for bacteriophage c2 infection of *Lactococcus lactis* subsp *lactis* C2. J. Bacteriol. **173:**6095–6100.
3. **Dupont K, Janzen T, Vogensen FK, Josephsen J, Stuer-Lauridsen B.** 2004. Identification of *Lactococcus lactis* genes required for bacteriophage adsorption. Appl. Environ. Microbiol. **70:**5825–5832.
4. **Randall-Hazelbauer L, Schwartz M.** 1973. Isolation of the bacteriophage lambda receptor from Escherichia coli. J. Bacteriol. **116:**1436–1446.
5. **Wang J, Michel V, Hofnung M, Charbit A.** 1998. Cloning of the J gene of bacteriophage lambda, expression and solubilization of the J protein: first in vitro studies on the interactions between J and LamB, its cell surface receptor. Res. Microbiol. **149:**611–624.
6. **Bonhivers M, Ghazi A, Boulanger P, Letellier L.** 1996. FhuA, a transporter of the Escherichia coli outer membrane, is converted into a channel upon binding of bacteriophage T5. EMBO J. **15:**1850–1856.
7. **Plançon L, Janmot C, le Maire M, Desmadril M, Bonhivers M, Letellier L, Boulanger P.** 2002. Characterization of a high-affinity complex between the bacterial outer membrane protein FhuA and the phage T5 protein pb5. J. Mol. Biol. **318:**557–569.
8. **Baptista C, Santos MA, Sao-Jose C.** 2008. Phage SPP1 reversible adsorption to Bacillus subtilis cell wall teichoic acids accelerates virus recognition of membrane receptor YueB. J. Bacteriol. **190:**4989–4996.
9. **Sao-Jose C, Lhuillier S, Lurz R, Melki R, Lepault J, Santos MA, Tavares**

P. 2006. The ectodomain of the viral receptor YueB forms a fiber that triggers ejection of bacteriophage SPP1 DNA. J. Biol. Chem. **281:**11464–11470.
10. **Yu F, Mizushima S.** 1982. Roles of lipopolysaccharide and outer membrane protein OmpC of Escherichia coli K-12 in the receptor function for bacteriophage T4. J. Bacteriol. **151:**718–722.
11. **Bartual SG, Otero JM, Garcia-Doval C, Llamas-Saiz AL, Kahn R, Fox GC, van Raaij MJ.** 2010. Structure of the bacteriophage T4 long tail fiber receptor-binding tip. Proc. Natl. Acad. Sci. U. S. A. **107:**20287–20292.
12. **Rossmann MG, Mesyanzhinov VV, Arisaka F, Leiman PG.** 2004. The bacteriophage T4 DNA injection machine. Curr. Opin. Struct. Biol. **14:**171–180.
13. **Leiman PG, Arisaka F, van Raaij MJ, Kostyuchenko VA, Aksyuk AA, Kanamaru S, Rossmann MG.** 2010. Morphogenesis of the T4 tail and tail fibers. Virol. J. **7:**355.
14. **Riede I.** 1987. Receptor specificity of the short tail fibres (gp12) of T-even type Escherichia coli phages. Mol. Gen. Genet. **206:**110–115.
15. **Bebeacua C, Bron P, Lai L, Vegge CS, Brondsted L, Spinelli S, Campanacci V, Veesler D, van Heel M, Cambillau C.** 2010. Structure and molecular assignment of lactococcal phage TP901-1 baseplate. J. Biol. Chem. **285:**39079–39086.
16. **Campanacci V, Veesler D, Lichiere J, Blangy S, Sciara G, Moineau S, van Sinderen D, Bron P, Cambillau C.** 2010. Solution and electron microscopy characterization of lactococcal phage baseplates expressed in Escherichia coli. J. Struct. Biol. **172:**75–84.
17. **Veesler D, Dreier B, Blangy S, Lichiere J, Tremblay D, Moineau S, Spinelli S, Tegoni M, Pluckthun A, Campanacci V, Cambillau C.** 2009. Crystal structure and function of a DARPin neutralizing inhibitor of lactococcal phage TP901-1: comparison of DARPin and camelid VHH binding mode. J. Biol. Chem. **284:**30718–30726.
18. **Veesler D, Spinelli S, Mahony J, Lichiere J, Blangy S, Bricogne G, Legrand P, Ortiz-Lombardia M, Campanacci V, van Sinderen D, Cambillau C.** 2012. Structure of the phage TP901-1 1.8 MDa baseplate suggests an alternative host adhesion mechanism. Proc. Natl. Acad. Sci. U. S. A. **109:**8954–8958.
19. **Deveau H, Labrie SJ, Chopin MC, Moineau S.** 2006. Biodiversity and classification of lactococcal phages. Appl. Environ. Microbiol. **72:**4338–4346.
20. **Kleppen HP, Bang T, Nes IF, Holo H.** 2011. Bacteriophages in milk fermentations: diversity fluctuations of normal and failed fermentations. Int. Dairy J. **21:**592–600.
21. **Castro-Nallar E, Chen H, Gladman S, Moore SC, Seemann T, Powell IB, Hillier A, Crandall KA, Chandry PS.** 2012. Population genomics and phylogeography of an Australian dairy factory derived lytic bacteriophage. Genome Biol. Evol. **4:**382–393.
22. **Moineau S, Borkaev M, Holler BJ, Walker SA, Kondo JK, Vedamuthu ER, Vandenbergh PA.** 1996. Isolation and characterization of lactococcal bacteriophages from cultured buttermilk plants in the United States. J. Dairy Sci. **79:**2104–2111.
23. **Rousseau GM, Moineau S.** 2009. Evolution of *Lactococcus lactis* phages within a cheese factory. Appl. Environ. Microbiol. **75:**5336–5344.
24. **Tremblay DM, Tegoni M, Spinelli S, Campanacci V, Blangy S, Huyghe C, Desmyter A, Labrie S, Moineau S, Cambillau C.** 2006. Receptor-binding protein of Lactococcus lactis phages: identification and characterization of the saccharide receptor-binding site. J. Bacteriol. **188:**2400–2410.
25. **Chapot-Chartier MP, Vinogradov E, Sadovskaya I, Andre G, Mistou MY, Trieu-Cuot P, Furlan S, Bidnenko E, Courtin P, Pechoux C, Hols P, Dufrene YF, Kulakauskas S.** 2010. Cell surface of Lactococcus lactis is covered by a protective polysaccharide pellicle. J. Biol. Chem. **285:**10464–10471.
26. **Ricagno S, Campanacci V, Blangy S, Spinelli S, Tremblay D, Moineau S, Tegoni M, Cambillau C.** 2006. Crystal structure of the receptor-binding protein head domain from *Lactococcus lactis* phage bIL170. J. Virol. **80:**9331–9335.
27. **Spinelli S, Campanacci V, Blangy S, Moineau S, Tegoni M, Cambillau C.** 2006. Modular structure of the receptor binding proteins of Lactococcus lactis phages. The RBP structure of the temperate phage TP901-1. J. Biol. Chem. **281:**14256–14262.
28. **Shepherd DA, Veesler D, Lichiere J, Ashcroft AE, Cambillau C.** 2011. Unraveling lactococcal phage baseplate assembly by mass spectrometry. Mol. Cell. Proteomics **10:**M111.009787. doi:10.1074/mcp.M111.009787.
29. **Bebeacua C, Lai L, Vegge CS, Brondsted L, van Heel M, Veesler D, Cambillau C.** 2013. Visualizing a complete Siphoviridae member by single-particle electron microscopy: the structure of lactococcal phage TP901-1. J. Virol. **87:**1061–1068.
30. **Sciara G, Blangy S, Siponen M, McGrath S, van Sinderen D, Tegoni M, Cambillau C, Campanacci V.** 2008. A topological model of the baseplate of lactococcal phage Tuc2009. J. Biol. Chem. **283:**2716–2723.
31. **Sambrook J, Russell DW.** 2001. Molecular cloning: a laboratory manual, 3rd ed.vol 1.Cold Spring Harbor Laboratory Press, Cold Spring Harbor, NY.
32. **Douillard FP, O'Connell-Motherway M, Cambillau C, van Sinderen D.** 2011. Expanding the molecular toolbox for Lactococcus lactis: construction of an inducible thioredoxin gene fusion expression system. Microb. Cell Fact. **10:**66.
33. **Horton RM, Cai ZL, Ho SN, Pease LR.** 1990. Gene splicing by overlap extension: tailor-made genes using the polymerase chain reaction. Biotechniques **8:**528–535.
34. **McGrath S, Neve H, Seegers JF, Eijlander R, Vegge CS, Brondsted L, Heller KJ, Fitzgerald GF, Vogensen FK, van Sinderen D.** 2006. Anatomy of a lactococcal phage tail. J. Bacteriol. **188:**3972–3982.
35. **Bradford MM.** 1976. Rapid and sensitive method for quantitation of microgram quantities of protein utilizing principle of protein-dye binding. Anal. Biochem. **72:**248–254.
36. **Tang G, Peng L, Baldwin PR, Mann DS, Jiang W, Rees I, Ludtke SJ.** 2007. EMAN2: an extensible image processing suite for electron microscopy. J. Struct. Biol. **157:**38–46.
37. **Shaikh TR, Gao H, Baxter WT, Asturias FJ, Boisset N, Leith A, Frank J.** 2008. SPIDER image processing for single-particle reconstruction of biological macromolecules from electron micrographs. Nat. Protoc. **3:**1941–1974.
38. **Scheres SH.** 2010. Classification of structural heterogeneity by maximum-likelihood methods. Methods Enzymol. **482:**295–320.
39. **Scheres SHW, Nunez-Ramirez R, Sorzano COS, Carazo JM, Marabini R.** 2008. Image processing for electron microscopy single-particle analysis using XMIPP. Nat. Protoc. **3:**977–990.
40. **van Heel M, Schatz M.** 2005. Fourier shell correlation threshold criteria. J. Struct. Biol. **151:**250–262.
41. **Pettersen EF, Goddard TD, Huang CC, Couch GS, Greenblatt DM, Meng EC, Ferrin TE.** 2004. UCSF Chimera—a visualization system for exploratory research and analysis. J. Comput. Chem. **25:**1605–1612.
42. **Garvey P, Hill C, Fitzgerald GF.** 1996. The lactococcal plasmid pNP40 encodes a third bacteriophage resistance mechanism, one which affects phage DNA penetration. Appl. Environ. Microbiol. **62:**676–679.
43. **Lillehaug D.** 1997. An improved plaque assay for poor plaque-producing temperate lactococcal bacteriophages. J. Appl. Microbiol. **83:**85–90.
44. **Kenny JG, McGrath S, Fitzgerald GF, van Sinderen D.** 2004. Bacteriophage Tuc2009 encodes a tail-associated cell wall-degrading activity. J. Bacteriol. **186:**3480–3491.
45. **Stockdale SR, Mahony J, Courtin P, Chapot-Chartier MP, van Pijkeren JP, Britton RA, Neve H, Heller KJ, Aideh B, Vogensen FK, van Sinderen D.** 2013. The lactococcal phages Tuc2009 and TP901-1 incorporate two alternate forms of their tail fiber into their virions for infection specialization. J. Biol. Chem. **288:**5581–5590.
46. **Chopin A, Deveau H, Ehrlich SD, Moineau S, Chopin MC.** 2007. KSY1, a lactococcal phage with a T7-like transcription. Virology **365:**1–9.
47. **Guo S, Shu D, Simon MN, Guo P.** 2003. Gene cloning, purification, and stoichiometry quantification of phi29 anti-receptor gp12 with potential use as special ligand for gene delivery. Gene **315:**145–152.
48. **Kuipers OP, de Ruyter PGGA, Kleerebezem M, de Vos WM.** 1998. Quorum sensing-controlled gene expression in lactic acid bacteria. J. Biotechnol. **64:**15–21.
49. **Costello VA.** 1988. Characterization of bacteriophage host interactions in Streptococcus cremoris UC503 and related lactic streptococci. Ph.D. thesis. National University of Ireland, University College Cork, Cork, Ireland.
50. **Christiansen B, Johnsen MG, Stenby E, Vogensen FK, Hammer K.** 1994. Characterization of the lactococcal temperate phage TP901-1 and its site-specific integration. J. Bacteriol. **176:**1069–1076.